Geosci. Model Dev. Discuss., 7, 7075–7119, 2014
www.geosci-model-dev-discuss.net/7/7075/2014/
doi:10.5194/gmdd-7-7075-2014


Geoscientific Model Development Discussions
Open Access



# A simple object-oriented and open source model for scientific and policy analyses of the global carbon cycle – Hector v0.1

**C. A. Hartin, P. Patel, A. Schwarber, R. P. Link, and B. P. Bond-Lamberty**

Pacific Northwest National Laboratory, Joint Global Change Research Institute at the University of Maryland–College Park, 5825 University Research Court, College Park, MD 20740, USA

Received: 14 August 2014 – Accepted: 29 September 2014 – Published: 24 October 2014

Correspondence to: C. A. Hartin (corinne.hartin@pnnl.gov)

Published by Copernicus Publications on behalf of the European Geosciences Union.

## Abstract

Simple climate models play an integral role in policy and scientific communities. They are used for climate mitigation scenarios within integrated assessment models, complex climate model emulation, and uncertainty analyses. Here we describe Hector v0.1, an open source, object-oriented, simple global climate carbon-cycle model. This model runs essentially instantaneously while still representing the most critical global scale earth system processes. Hector has three main carbon pools: an atmosphere, land, and ocean. The model's terrestrial carbon cycle includes respiration and primary production, accommodating arbitrary geographic divisions into, e.g., ecological biomes or political units. Hector's actively solves the inorganic carbon system in the surface ocean, directly calculating air–sea fluxes of carbon and ocean pH. Hector reproduces the global historical trends of atmospheric [$CO_2$] and surface temperatures. The model simulates all four Representative Concentration Pathways with high correlations ($R > 0.7$) with current observations, MAGICC (a well-known simple climate model), and the Coupled Model Intercomparison Project version 5. Hector is freely available under an open source license, and its modular design will facilitate a broad range of research in various areas.

## 1 Introduction

Projecting future impacts of anthropogenic perturbations on the climate system relies on understanding the interactions of key earth system processes. To accomplish this, a hierarchy of climate models with differing levels of complexity and resolution are used, ranging from simple energy balance models to fully-coupled atmosphere–ocean-general circulation models (AOGCMs) (Stocker, 2011).

Simple climate models (SCMs) represent only the most critical global scale earth system processes with low spatial and temporal resolution, e.g., carbon fluxes between the ocean and atmosphere, and respiration and primary production on land.





GMDD
7, 7075–7119, 2014

These models are relatively easy to use and understand, and are computationally inexpensive. Most SCMs have a few key features: (1) calculating future concentrations of greenhouse gases (GHGs) from given emissions, (2) calculating global mean radiative forcing from concentrations, (3) converting the radiative forcing to global mean temperature, and (4) modeling the carbon cycle, an essential part of the climate system (e.g., Wigley, 1991; Meinshausen et al., 2011a; Tanaka et al., 2007b; Lenton, 2000).

With these capabilities, SCMs play an integral role in policy and scientific research. For example, energy-economic-climate models or Integrated Assessment Models (IAMs) are used to address issues on energy system planning, climate mitigation and stabilization pathways, land-use changes, pollution control, and population policies (Wigley et al., 1996; Edmonds and Smith, 2006; van Vuuren et al., 2011c). AOGCMs are too computationally expensive to use in these analyses. Therefore all IAMs have a simple representation of the global climate system in which emissions data from the IAMs are converted to concentrations and then radiative forcing and global temperature are calculated.

SCMs are also used as emulators of more complex AOGCMs (e.g., Meinshausen et al., 2011a, c; Schlesinger and Jiang, 1990; Challenor, 2012; Ratto et al., 2012). The components of SCMs can be constrained to replicate the overall behavior of the more complex model components. For instance, the climate sensitivity of a SCM can be made equal to that of an AOGCM by altering a single model parameter. One SCM, MAGICC, has been central to the analyses presented in the Intergovernmental Panel on Climate Change (IPCC) reports, emulating a large suite of AOGCMs (Meinshausen et al., 2011a).

Lastly, SCMs are computationally efficient and inexpensive to run, and therefore are used for run multiple simulations of future climate change emissions scenarios, parameter sensitivity experiments, perturbed physics experiments, large ensemble runs, and uncertainty analyses (Senior and Mitchell, 2000; Hoffert et al., 1980; Harvey and Schneider, 1985; Ricciuto et al., 2008; Sriver et al., 2012; Irvine et al., 2012). SCMs are fast enough that multiple scenarios can be simulated, and a wide range of parameter values can be tested. Specifically, SCMs have been useful in reducing uncertainties in future $CO_2$ sinks, quantifying parametric uncertainties in sea-level rise, ice-sheet modeling, ocean-heat uptake, and aerosol forcings (Ricciuto et al., 2008; Sriver et al., 2012; Applegate et al., 2012; Urban and Keller, 2009).

This study introduces Hector v0.1, object-oriented, simple climate carbon-cycle model. Hector is open source, an important quality given that the scientific community, funding agencies, and journals are increasingly emphasizing transparency and open source (E.P. White, 2013; Heron et al., 2013). With an open source model a large community of scientists can access, use, and enhance it, with the potential for long-term utilization and reproducibility (Ince et al., 2012).

One of the basic questions faced in developing a SCM is how much detail should be represented in the climate system. Our goal is to introduce complexity only where warranted, keeping the representations of the climate system as simple as possible. This results in fewer calculations, faster execution times, and easier analysis and interpretation of results. Sections 2, 3, and 4 describe the structure and components of Hector. Sections 5 and 6 describe the experiments, results and comparison of Hector against other models (MAGICC and CMIP5).

## 2 Model architecture

### 2.1 Overall structure and design

Hector is written in C++ and uses an object-oriented design that enforces clean separation between its different parts, which interact via strictly defined interfaces. The separation keeps each software module self-contained, which makes the code easy for users to understand, maintain, and enhance. Entities in the model include a command-line *wrapper*, the model *coupler*, various *components* organized around scientific areas (carbon cycling, radiative forcing, etc.) and *visitors* responsible for model output. Each of these is discussed below.





GMDD
7, 7075–7119, 2014

## 2.2 Model coupler

Hector's control flow starts with the coupler, which is responsible for: (1) parsing and routing input data to the model components, (2) tracking how the components depend on each other, (3) passing messages and data between components, (4) providing facilities for logging, time series interpolation, etc., and (5) controlling the main model loop as it progresses through time. Any errors thrown by the model are caught by the wrapper, which prints a detailed summary of the error.

Input data are specified in flat text files, and during startup are routed to the correct model component for its initialization. Some of the key initial model conditions are summarized in Tables 1 and 2. For more details of initial model conditions we urge the reader to download Hector v0.1 (https://github.com/JGCRI/hector). Components can send messages to each other during the model run, most often requesting data. The coupler handles message routing (via the *capability* mechanism, below) and enforces mandatory type checking: e.g., if a component requests mean global temperature in °C but the data are provided in K, an error will be thrown (i.e., execution halts) unless the receiving component can handle this situation.

Visitor patterns are units of code that traverse all model components and handle model output (Martin et al., 1997). Two visitors currently exist: one saves an easily-readable summary table to an output file, while the other writes a stream of model data (both standard outputs and internal diagnostics). After the model is finished running, this "stream" file can be parsed and summarized by R scripts included with the code (R Development Core Team, 2014). Log files may also be written by any model entity, using facilities provided by the coupler. The full sequence of events during a model run is summarized in Fig. 1.

## 2.3 Components

Model components are submodels that communicate with the coupler. From the coupler's point of view, components are fully defined by their *capabilities* and *dependencies*. At model startup, before the run begins, components inform the coupler of their capabilities, i.e., what data they can provide to the larger model system. The coupler uses this information to route messages between components, such as requests for data. Components register their dependencies, i.e., what data they require in order for their computations. After initialization, but before the model begins to run, the coupler uses this dependency information to determine the order in which components will be called in the main control loop.

The model's modular architecture, and the *capability/dependency* systems described above, allows swapping, enabling and disabling of model components directly via the input without recompiling. For example, this means that a user can test two different ocean submodels and easily compare results without having to rebuild the model.

### 2.4 Time step, spinup, and constraints

The model's fundamental time step is 1 year, although the carbon cycle can operate on a finer resolution when necessary (Sect. 2.6.1). When the model is on an integer date (e.g. 1997.0) it is considered to be the midpoint of that particular calendar year, in accordance with Representative Concentration Pathway (RCP) data (Meinshausen et al., 2011b).

Like many models, Hector has an optional "spinup" step, in which the model runs to equilibrium in an ahistorical, perturbation-free mode (Pietsch and Hasenauer, 2006). This occurs after model initialization, but before the historical run begins, and ensures that the model is in steady state when it enters the main simulation. During spinup, the coupler repeatedly calls all the model components in their dependency-driven ordering, using an annual time step. Each component signals whether it needs further steps to stabilize, and this process repeats until all components signal that they are complete.

Currently only the model's carbon cycle makes use of spinup. Spinup takes place prior to land use change or industrial emission inputs. The main carbon cycle moves from its initial, user-defined carbon pool values to a steady state in which $\delta C/\mathrm{d}t < \varepsilon$



Discussion Paper | Discussion Paper | Discussion Paper | Discussion Paper |
GMDD
7, 7075–7119, 2014

for all pools; the convergence criterion $\varepsilon$ is user-definable and by default $1\,\mathrm{Tg\,C\,yr^{-1}}$. From its default values the preindustrial carbon cycle will typically stabilize in 300–400 time steps.

The model can be constrained, i.e., matching its output to a user-supplied time series, to allow isolation and testing of different components. Available constraints currently include atmospheric $CO_2$, global temperature anomaly, total ocean–atmosphere carbon exchange, total land–atmosphere carbon exchange, and total radiative forcing. Most constraints operate by overwriting model-calculated values with user-supplied time series data during the run. The atmospheric [$CO_2$] constraint operates slightly differently, as the global carbon cycle is subject to a continuous mass-balance check. As a result, when the user supplies a [$CO_2$] record between arbitrary dates and orders the model to match it, the model *computes* [$CO_2$] at each time step, and any deficit (surplus) in comparison with the constraint [$CO_2$] is drawn from (added to) the deep ocean. The deep ocean holds the largest reservoir of carbon; therefore, small changes in this large pool have a negligible effect on the carbon cycle dynamics. When the model exits the constraint time period, [$CO_2$] again becomes fully prognostic.

### 2.5 Code availability and dependencies

All Hector code is open source and available at https://github.com/JGCRI/hector. The repository includes model code that can be compiled on Mac, Linux, and Windows, inputs files for the four Representative Concentration Pathways (RCP) cases discussed in Sect. 4, R scripts to process model output, and documentation. We kept the dependencies as limited as possible, with only the GNU Scientific Library (GSL, Gough, 2009) and the Boost C++ libraries (http://www.boost.org). An optional unit testing build target requires the googletest framework (http://code.google.com/p/googletest). However, this is not needed to compile and run Hector. HTML documentation can be automatically generated from the code using the Doxygen tool (http://www.doxygen.org). All these tools and libraries are free and open source.





GMDD
7, 7075–7119, 2014

## 3 Main carbon cycle

In the model's default terrestrial carbon cycle, terrestrial vegetation, detritus, and soil are linked with each other and the atmosphere by first-order differential equations (Fig. 2). Vegetation net primary production is a function of atmospheric [$CO_2$] and temperature. Carbon flows from the vegetation to detritus and then soil, losing fractions to heterotrophic respiration on the way. Land-use emissions are specified as inputs. An "earth" pool debits carbon emitted as anthropogenic emissions, allowing a continual mass-balance check across the entire carbon cycle.

More formally, any change in atmospheric carbon, and thus [$CO_2$], occurs as a function of anthropogenic emissions, land-use change emissions, and the atmosphere–ocean carbon flux. The atmosphere is treated as a single well-mixed box whose rate of change is:

$$\frac{\mathrm{d}C_{\mathrm{atm}}}{\mathrm{d}t} = F_{\mathrm{A}}(t) + F_{\mathrm{LC}}(t) - F_{\mathrm{O}}(t) - F_{\mathrm{L}}(t) \tag{1}$$

where, $F_A$ is the anthropogenic emissions, $F_{LC}$ is the land use change emissions and $F_O$ and $F_L$ are the atmosphere ocean and atmosphere land fluxes. The overall terrestrial carbon balance at time $t$ is the difference between net primary production (NPP) and heterotrophic respiration (RH). This is summed over user-specified $n$ groups (each typically regarded as a latitude band, biome, or -political units), with $n \geq 1$:

$$F_L(t) = \sum_{i=1}^{n} \mathrm{NPP}_i(t) - \mathrm{RH}_i(t) \tag{2}$$

Note that NPP here is assumed to include disturbance effects, for which there is currently no separate term. For each biome $i$, NPP and RH are computed as functions of their preindustrial values $\mathrm{NPP}_0$ and $\mathrm{RH}_0$, current atmospheric carbon $C_{\mathrm{atm}}$, and the





GMDD
7, 7075–7119, 2014

biome's temperature anomaly $T_i$:

$$\mathrm{NPP}_i(t) = \mathrm{NPP}_0 \cdot f(C_{\mathrm{atm}}, \beta_i) \tag{3}$$

$$f(C_{\mathrm{atm}}, \beta_i) = 1 + \beta_i (C_{\mathrm{atm}}/C_0) \tag{4}$$

$$\mathrm{RH}_i(t) = \mathrm{RH}_0 \times Q_{10i}^{T_i(t)/10} \tag{5}$$

$$T_i(t) = T_G(t) \times \delta_i \tag{6}$$

These are commonly used formulations: NPP is modified by a the user-specified carbon fertilization parameter, $\beta$ (Piao et al., 2013). RH changes are controlled by a biome-specific $Q_{10}$ value. Biomes can experience temperature changes at rates that differ from the global mean $T_{\mathrm{G}}$, controlled by a user specified temperature factor $\delta_I$.

Land carbon pools (vegetation, detritus, and soil) change as a result of NPP, RH, and land-use change fluxes, whose effects are partitioned among these carbon pools. In addition, carbon flows from vegetation to detritus and soil (Fig. 2). Partitioning fractions ($f$) control the flux quantities between pools (Table 2). For simplicity Eqs. (8)–(10) omit the time $t$ and biome-specific $i$ notations, but each pool is tracked separately for each biome at each time step:

$$\frac{\mathrm{d}C_{\mathrm{V}}}{\mathrm{d}t} = \mathrm{NPP}\, f_{\mathrm{nv}} - C_{\mathrm{V}}(f_{\mathrm{vd}} + f_{\mathrm{vs}}) - F_{\mathrm{LC}} f_{\mathrm{lv}} \tag{7}$$

$$\frac{\mathrm{d}C_{\mathrm{D}}}{\mathrm{d}t} = \mathrm{NPP}\, f_{\mathrm{nd}} + C_{\mathrm{V}} f_{\mathrm{vd}} - C_{\mathrm{D}} f_{\mathrm{ds}} - \mathrm{RH}\, f_{\mathrm{rd}} - F_{\mathrm{LC}} f_{\mathrm{ld}} \tag{8}$$

$$\frac{\mathrm{d}C_S}{\mathrm{d}t} = \mathrm{NPP}\, f_{\mathrm{ns}} + C_{\mathrm{V}} f_{\mathrm{vs}} + C_{\mathrm{D}} f_{\mathrm{ds}} - \mathrm{RH}\, f_{\mathrm{rs}} - F_{\mathrm{LC}} f_{\mathrm{ls}} \tag{9}$$

The ocean–atmosphere carbon flux is the sum of the ocean's surface fluxes (currently $n = 2$, high and low latitude surface box):

$$F_O(t) = \sum_{i=1}^{n} F_i(t) \tag{10}$$





GMDD
7, 7075–7119, 2014

The surface fluxes of each individual box are calculated from an ocean chemistry model described in detail by Hartin et al. (2014) based on equations from Zeebe and Wolf-Gladrow, (2001). The flux of $CO_2$ for each box $i$ is calculated by:

$$F_i(t) = k\alpha\Delta pCO_2 \tag{11}$$

Where $k$ is the $CO_2$ gas-transfer velocity, $\alpha$ is the solubility of $CO_2$ in water based on salinity, temperature, and pressure, and $\Delta pCO_2$ is the atmosphere–ocean gradient of $pCO_2$ (Takahashi et al., 2009). At steady state, the cold high latitude surface box ($> 55^\circ$, subpolar gyres) acts as a sink of carbon from the atmosphere, while the warm low latitude surface box ($< 55^\circ$) off gases carbon back to the atmosphere. Temperatures of the surface boxes are linearly related to atmospheric global temperatures (see Sect. 4.1), $T_{HL} = \Delta T - 13$ and $T_{LL} = \Delta T + 7$ (Lenton, 2000). The ocean model, modeled after Lenton et al. (2000) and Knox and McElroy (1984), circulate carbon through four boxes (two surface, one intermediate depth, one deep), via water mass advection and exchange, simulating a simple thermohaline circulation (Fig. 2). At steady state, approximately 100 Pg of carbon are transferred from the high latitude surface box to the deep box based on the volume of the box and transport in Sv ($10^6\,m^3\,s^{-1}$) between the boxes. The change in carbon of any box $i$ is given by the fluxes in and out:

$$\frac{dC_i}{dt} = \sum_{j=1}^{in} F_{j\to i} - \sum_{j=1}^{out} F_{i\to j} + F_i \tag{12}$$

As the model advances, the carbon values or DIC change in each box. The new DIC values are used within the chemistry submodel to calculate $pCO_2$ values at the next time step.

### 3.1 Adaptive-time step solver

The fundamental time step in Hector is currently one year, and most model components are solved at this resolution. The carbon cycle, however, can operate on a variable time step, helping to stabilize it under particularly high-emissions scenarios. This will also allow future sub-annual applications where desired. The adaptive time step accomplished using the *gsl_odeiv2_evolve_apply* solver package of GSL 1.16, which attempts many different step sizes to reliably (i.e., with acceptable error) advance the model. Thus all the carbon cycle components handle indeterminate time steps ≤ 1 yr, and can signal the solver if a too-large time step is leading to instability. The solver then re-retries the solution, using a series of smaller steps. From the coupler's point of view, however, the entire model continues to advance in annual increments.

## 4 Other components

### 4.1 Global atmospheric temperature

Near surface global atmospheric temperature is calculated by:

$$\Delta T(t) = \lambda \times \mathrm{RF}(t) - F_\mathrm{H}(t) \tag{13}$$

where, user-specified $\lambda$ is the climate feedback parameter, defined as $\lambda = S'/S$, where $S'$ is the climate sensitivity parameter (3 K) and $S$ is the equilibrium climate sensitivity for a doubling of $CO_2$ (3.7 W m$^{-2}$) (Knutti and Hegerl, 2008). RF is the total radiative forcing and $F_\mathrm{H}$ is the ocean heat flux. $F_\mathrm{H}$ is calculated by a simple expression of the ocean heat uptake efficiency $k$ (W m$^{-2}$ K$^{-1}$) and the atmospheric temperature change prior to the ocean's removal of heat from the atmosphere (Raper et al., 2002):

$$\Delta F_\mathrm{H}(t) = k \times \Delta T(t) \tag{14}$$

### 4.2 Radiative forcing

Radiative forcing is calculated from a series of atmospheric greenhouse gases, aerosols, and pollutants (Eqs. 17, 19–25, 27). Radiative forcing is reported as the relative radiative forcing. The base year user-specified forcings are subtracted from the total radiative forcing to yield a forcing relative to the base year. In the current model of Hector, the gases other than $CO_2$ are only used for the calculation of radiative forcing.





GMDD
7, 7075–7119, 2014

#### 4.2.1 Halocarbons

The halocarbon component of the model can accept an arbitrary number of gas species, each characterized by a name, a lifetime $\tau$ (yr), a radiative forcing efficiency $\rho$ ($W\,m^{-2}\,pptv^{-1}$), a user-specified preindustrial concentration (pptv), and a molar mass (g). For each gas, its concentration ($C_i$) at time $t$ is then computed based on a specified emissions time series $E$, assuming an exponential decay from the atmosphere:

$$C_i(t) = C_i(t-1)\left(1 - \frac{1}{\tau}\right) + E_i(t) \quad (15)$$

The default model input files include these parameters and a time series of emissions for C2F6, CCl4, CF4, CFC11, CFC12, CFC113, CFC114, CFC115, CH3Br, CH3CCl3, CH3Cl, HCF22, HCF141b, HCF142b, HFC23, HFC32, HFC125, HFC134a, HFC143a, HFC227ea, HFC245ca, HFC245fa, HFC4310, SF6, halon1211, halon1301, and halon2402.

Radiative forcing by halocarbons, other gases controlled under the Montreal Protocol, $SF_6$, and ozone are calculated via:

$$\mathrm{RF} = \alpha[C(t) - C(t_0)] \quad (16)$$

where $\alpha$ is the radiative efficiency in $W\,m^{-2}\,ppbv^{-1}$, and $C$ is the atmospheric concentration.





GMDD
7, 7075–7119, 2014

#### 4.2.2 Ozone

Tropospheric ozone concentrations are calculated by the $CH_4$ concentration and the emissions of three primary pollutants: $NO_x$, CO, and NMVOCs:

$$\begin{aligned} O_3(t) = O_3(2000) + 5.0\ln\left[\frac{CH_4(t)}{CH_4(2000)}\right] &+ 0.125[eNO_x(t) - eNO_x(2000)] \\ &+ 0.0011[eCO(t) - eCO(2000)] \\ &+ 0.0033[eVOC(t) - eVOC(2000)] \end{aligned} \quad (17)$$

where the constants are the ozone sensitivity factors for each of the precursors (Ehhalt et al., 2001). The radiative forcing of tropospheric ozone is calculated from a linear relationship using a radiative efficiency factor (Joos et al., 2001) and a pre-industrial value of ozone of 25 DU (IPCC, 2001):

$$RF_{O_3} = 0.042\,\mathrm{W\,m^{-2}DU^{-1}} \times [[O_3] - [O_3]\mathrm{pre}] \quad (18)$$

#### 4.2.3 BC and OC

The radiative forcing from black carbon is a function of the black carbon and organic carbon emissions ($e$BC and $e$OC).

$$RF_{BC} = 0.0743 \times 10^{-9}\,\mathrm{W\,m^{-2}\,kg^{-1}} \times e\mathrm{BC} \quad (19)$$

$$RF_{OC} = -0.0128 \times 10^{-9}\,\mathrm{W\,m^{-2}\,kg^{-1}} \times e\mathrm{OC} \quad (20)$$

The coefficients $0.0743 \times 10^{-9}$ and $-0.0128 \times 10^{-9}$ include both indirect and direct forcings of black and organic carbon (fossil fuel and biomass) (Bond et al., 2013).





GMDD
7, 7075–7119, 2014

#### 4.2.4 Sulphate aerosols

The radiative forcing from sulphate aerosols is a combination of the direct and indirect forcings (Joos et al., 2001).

$$\mathrm{RF}_{\mathrm{SO_x\ Direct}} = -0.4\,\mathrm{W\,m^{-2}} \times \frac{e\mathrm{SO_x}(t)}{e\mathrm{SO_x}(2000)} \tag{21}$$

$$\mathrm{RF}_{\mathrm{SO_x\ Indirect}} = -0.8\,\mathrm{W\,m^{-2}} \times \frac{(\ln(e\mathrm{SN}) + e\mathrm{SO_x}(t))}{e\mathrm{SN}} \times \left(\ln \frac{e\mathrm{SN} + e\mathrm{SO_x}(2000)}{e\mathrm{SN}}\right)^{-1} \tag{22}$$

The direct forcing by sulphate aerosols is proportional to the anthropogenic sulphur emissions ($\mathrm{GgS\,yr^{-1}}$) divided by the sulphate emissions from 2000. The indirect forcing by sulphate aerosols is a function of the anthropogenic and natural sulphur emissions. Natural sulphur emissions denoted by $e$SN is equal to 42 000 GgS. A time series of annual mean volcanic stratospheric aerosol forcing ($\mathrm{W\,m^{-2}}$) is supplied from Meinshausen et al. (2011b) and is added to the indirect and direct forcing for a total sulphate forcing.

#### 4.2.5 $N_2O$ and $CH_4$

The radiative forcing equations for $CH_4$ and $N_2O$ (Joos et al., 2001) are a function of the concentrations (ppbv) and their radiative efficiency:

$$\begin{aligned}\mathrm{RF}_{\mathrm{CH_4}} = {} & 0.036\,\mathrm{W\,m^{-2}} \left[\sqrt{\mathrm{CH_4}(t)} - \sqrt{\mathrm{CH_4}(t_0)}\right] \\ & - f[\mathrm{CH_4}(t), \mathrm{N_2O}(t_0)] - f[\mathrm{CH_4}(t_0), \mathrm{N_2O}(t_0)]\end{aligned} \tag{23}$$

$$\begin{aligned}\mathrm{RF}_{\mathrm{N_2O}} = {} & 0.12\,\mathrm{W\,m^{-2}} \left[\sqrt{\mathrm{N_2O}(t)} - \sqrt{\mathrm{N_2O}(t_0)}\right] \\ & - f[\mathrm{CH_4}(t_0), \mathrm{N_2O}(t)] - f[\mathrm{CH_4}(t_0), \mathrm{N_2O}(t_0)]\end{aligned} \tag{24}$$





GMDD
7, 7075–7119, 2014
A simple open source model for analyses of the global carbon cycle – Hector v0.1
C. A. Hartin et al.

Title Page
Abstract | Introduction
Conclusions | References
Tables | Figures
◂◂ | ▸▸
◂ | ▸
Back | Close
Full Screen / Esc
Printer-friendly Version
Interactive Discussion

The function $f$ accounts for the overlap in $CH_4$ and $N_2O$ in their bands is:

$$f(M,N) = 0.47 \times \ln(1 + (2.01 \times 10^{-5}) \times (MN)^{0.75} + (5.31 \times 10^{-15}) \times M \times (MN)^{1.52}) \quad (25)$$

Note, we are not explicitly calculating concentrations of $CH_4$ and $N_2O$ within Hector, instead we have input files of concentrations.

#### 4.2.6 Stratospheric $H_2O$ from $CH_4$ oxidation

The radiative forcing from stratospheric $H_2O$ is a function of the $CH_4$ concentrations (Tanaka et al., 2007a). The coefficient 0.05 is from Joos et al. (2001) based on the fact that the forcing contribution from stratospheric $H_2O$ is about 5 % of the total $CH_4$ forcing (IPCC, 2001). The 0.036 coefficient corresponds to the same coefficient used in the $CH_4$ radiative forcing equation.

$$RF_{stratH_2O} = 0.05 \times \left\{0.036\,\mathrm{W\,m^{-2}} \times \left(\sqrt{[CH_4]_t} - \sqrt{[CH_4]_{t_0}}\right)\right\} \quad (26)$$

## 5 Model experiments and data sources

A critical test of Hector's performance is to compare the major climatic variables calculated in Hector, e.g., atmospheric $[CO_2]$, radiative forcing, and atmospheric temperature, to observational records and other models. We run Hector under historical conditions from 1850–2005 and then under all four Representative Concentration Pathways (RCPs) out to 2300 (Moss et al., 2010). The RCPs are plausible future scenarios that are developed to improve our understanding of the coupled human climate system. All necessary emission and concentration inputs are from the four RCPs (RCP 2.6, RCP 4.5, RCP 6.0 and RCP 8.5) freely available at http://www.pik-potsdam.de/~mmalte/rcps/ (Meinshausen et al., 2011b; Riahi et al., 2011; van Vuuren et al., 2011a, b, d; Masui et al., 2011; Thomson et al., 2011).





GMDD
7, 7075–7119, 2014
A simple open source model for analyses of the global carbon cycle – Hector v0.1
C. A. Hartin et al.

Comparison data is obtained from a series of models. We compared Hector results to MAGICC, a SCM widely used in the scientific and IAM communities, for global variables such as atmospheric $CO_2$, radiative forcing, and temperature (e.g., Raper et al., 2001; Wigley, 1995; Meinshausen et al., 2011a). We also compare Hector to a suite of eleven Earth System Models included in the Coupled Model Intercomparison Project (CMIP5) archive (Taylor et al., 2012) (Table 3). All CMIP5 data are converted to yearly global averages from the historical period through the RCPs and their extensions. One SD and the CMIP5 model spread is calculated for each variable. All CMIP5 variables used in this study are from model runs with prescribed atmospheric concentrations, except for comparisons involving atmospheric [$CO_2$] which are from the emissions driven scenario (esmHistorical and esmRCP8.5). The models that run esmRCP8.5 are typically earth system models used to investigate the carbon cycle in further detail.

Lastly, we compare Hector to observations of atmospheric [$CO_2$] concentrations from Law Dome (1010–1975) and Mauna Loa (1958–2008), (Keeling and Whorf, 2005; Etheridge et al., 1996). Global temperature anomalies are from HadCRUT4 (Morice et al., 2012). Observations of air–sea and air–land fluxes are from the Global Carbon Project (GCP) (Le Quéré et al., 2013). Lastly, observations of surface ocean pH are from Bermuda Atlantic Time Series (BATS) and Hawaii Ocean Time Series (HOTS) (Bates, 2007; Fujieki et al., 2013).

## 6 Results and discussion

### 6.1 Historical

A critical test of Hector's performance is how well it compares to historical and present day climate from observations, MAGICC, and a suite of CMIP5 models. We carried out a few statistical tests on Hector (e.g., correlation and root mean square error) which are summarized in Table 4. After spinup is complete in Hector, the atmospheric [$CO_2$] in 1850 is 286.0 ppmv, comparing well with observations from Law Dome of 285.2 ppmv.

Compared to observations, MACGICC6, and CMIP5 data from 1850 to 2004, Hector captures the global trends in atmospheric [$CO_2$] (Fig. 3) with correlation coefficients of $R > 0.99$ and an average root mean square error (RMSE) of 2.6 ppmv (Table 4a). Hector has the ability to match atmospheric [CO2] records, but we disabled this feature to highlight the full performance of the model.

Historical global atmospheric temperature anomalies (relative to 1850) are compared across Hector, MAGICC6, CMIP5, and observations from HadCRUT4 (Fig. 4). Hector is running without the effects of volcanic forcing, leading to the smoother representation of temperature with time. Atmospheric temperature change from Hector over the period 1850 to 2004 is well correlated to (> 0.8) to observations and models with an average RMSE of 0.12 °C.

## 6.2 Future projections

Within the modeling community, models that best simulate the historical and present day climate are assumed to be credible under future projections. We are confident in Hector's ability to reproduce historical trends and are therefore confident in its ability to simulate future climate changes. We compare Hector to MAGICC and CMIP5 under differing future climate projections.

Figure 5 highlights historical trends in atmospheric [$CO_2$], along with projections of atmospheric [$CO_2$] under esmRCP8.5 from 1850 to 2100. Hector is perfectly correlated with MAGICC and CMIP5 over this period and with a RMSE of 9.2 ppmv (Table 4b). Hector and MAGICC6 diverge from the CMIP5 median most notably after 2050, but are both still within the low end of the CMIP5 model spread.

Figure 6 compares atmospheric [$CO_2$] from Hector and MAGICC6 under all four RCP scenarios out to 2300. Hector is well correlated with MAGICC6 from 1850 out to 2300 for the four RCPs. Under all of the scenarios except for RCP 8.5, atmospheric [$CO_2$] within Hector fluctuates around the MAGICC6 atmospheric [$CO_2$] values, with the most notable fluctuations under low carbon emissions. This is due to changes in the flux





GMDD
7, 7075–7119, 2014

of carbon over the land as net primary production and respiration change with $CO_2$ fertilization and temperature effects.

We compare Hector to MAGICC6 for changes in radiative forcing under the four RCPs (Fig. 7). Radiative forcing is not an output from the CMIP5 models and therefore we can only compare Hector and MAGICC6. Hector is offset slightly lower compared to MAGICC6, which is expected since atmospheric [$CO_2$] is slightly lower. Over the period 1850 to 2300 Hector is well correlated (1.0) with MAGICC6 with a RMSE of 0.25 $W\,m^{-2}$. We acknowledge that the correlation is lower under the historical period (0.79). This may be due to slight differences in the representation of atmospheric gases, pollutants, and aerosols between the two models.

Figure 8 compares global temperature anomalies from Hector to MAGICC6 and CMIP5 over the four RCPs, from 2005 to 2300. Hector and MAGICC6 are comparable in their temperature change across the four RCPs. However, both are lower than the CMIP5 median under RCP 2.6, 4.5 and 8.5, with the largest discrepancy under high $CO_2$ emissions in RCP 8.5. Regardless, Hector is still highly correlated (> 0.97) to MAGICC6 and CMIP5 for RCP 8.5, with a RMSE of 0.52 °C compared to CMIP5 (Table 4c). The fluctuations seen in RCP 2.6 within atmospheric [$CO_2$] are also apparent in the atmospheric temperature trends. However, the general trends of temperature change, peaking around 2050 and then slowly declining out to 2300 are captured within Hector.

Another way to visualize model performance is a Taylor diagram (Fig. 9) of global temperature change relative to 1850, from 1850 to 2300 for RCP 8.5. The closer the points are to the reference point (Hector) the higher the correlation and low RMSE between CMIP5 models and MAGICC6. Those points with a SD similar to that of Hector experience the same amplitude of temperature change over this time period (MAGICC6). All of the models are highly correlated with Hector, with a large range in the SD (1–5 °C).

Figures 10 and 11 present a detailed view of carbon fluxes under RCP 8.5, for CMIP5 and observations. The ocean is a major sink of carbon through 2100, becoming less





GMDD
7, 7075–7119, 2014

effective with time in both Hector and the CMIP5 models. MAGICC6 does not include air–sea fluxes in its output, and because it is not open source we were unable to obtain these values. Therefore, we compare air–sea fluxes of $CO_2$ to MAGICC5.3, the version currently used in the IA model, Global Change Assessment Model, updated with explicit BC and OC forcing as described in Smith and Bond (2014). The correlation is high between Hector and CMIP5 over the historical period (0.95). However, the correlation drops off significantly between 2005 and 2300 (0.10) (Table 4c). This is an active area of research, investigating the differences between Hector and CMIP5 after 2100. One potential reason for the low correlation after 2100 could be due to the fact that we are only comparing to three models that run the RCP extension to 2300 (bcc-csm1-1, IPSL-CM5A-LR, and MPI-ESM-LR). With a larger spread of fluxes, Hector may be better correlated. The average correlation over the CMIP5 models over 1850–2300 is higher at 0.80, with a RMSE of 1.45 Pg C $yr^{-1}$ (Table 4b). The land fluxes have a large range of uncertainty into the future within the CMIP5 models. Hector follows the general trends of the land acting as a sink of carbon initially with a gradual switch to a carbon source after 2150. Fluxes of carbon over the land are less well correlated to the CMIP5 median compared to the air–sea fluxes, 0.55 (historical) and 0.65 (RCP 8.5). Both land and ocean fluxes within Hector agree well the observations from LeQuere et al., (2013).

Lastly, a unique feature of Hector is its ability to actively solve the carbonate system in the upper ocean. This feature allows us to predict ocean acidification, calcium carbonate saturations and other parameters of the carbonate system. Figure 12 shows low latitude ($< 55$) pH for Hector compared to CMIP5 and observations from 1850 to 2100 under RCP 8.5. We see a significant drop in pH from present day through 2100.

## 7 Conclusions

Hector reproduces the large scale couplings and feedbacks on the climate system between the atmosphere, ocean, and land. Hector falls within the range of the CMIP5 model spread and tracks well with MAGICC. Our goal was not to simulate the fine





GMDD
7, 7075–7119, 2014

details or parameterizations typically found in large scale complex models, but instead to represent only the most critical global processes. This allows for fast execution times, ease of understanding and straightforward analysis of the model output. To help with the analysis of Hector we included within the online database of Hector, R scripts to process Hector's output as well as the comparison data.

Hector's two key features are its open source license and modular design. This allows the user to manipulate the input files, enable/disable/replace components, or include components not found within the core version of Hector. For example, the user can design a new submodel (e.g., sea-ice) to answer specific climate questions relating to that process. Because of these critical features, Hector has the potential to be a key analytical tool in both the policy and scientific communities. We welcome user input and encourage use, modifications, and collaborations with Hector.

While Hector has many strengths, there are a few limitations that later versions of Hector hope to address. For example, Hector does not have differential radiative forcing and atmospheric temperature calculations over land and ocean. The land responds to changes in emissions of greenhouse gases, and aerosols much quicker than the ocean, leading to different temperature responses over the land and ocean. Also, Hector does not explicitly deal with oceanic heat uptake. Surface temperatures are calculated based on a linear relationship with atmospheric temperature and heat uptake by the ocean is parameterized by a constant heat uptake efficiency. While Hector can reproduce global trends in atmospheric $CO_2$, and temperature, we cannot investigate ocean heat uptake in the deep ocean using Hector. Currently, there is placeholder in Hector for a more sophisticated sea-level rise submodel. The current edition of Hector uses inputs of concentrations of $CH_4$ and $N_2O$ to calculate radiative forcing from $CH_4$ and $N_2O$. Ideally we would like Hector to calculate concentrations from emissions of $CH_4$ and $N_2O$. This would allow for quick integration within IAMs.

Future plans with Hector include addressing some of the above limitations and conducting numerous scientific experiments, using Hector as a stand-alone simple climate carbon-cycle model. Also, Hector will be incorporated into Pacific Northwest National





GMDD
7, 7075–7119, 2014

Laboratory's Global Change Assessment Model to begin running policy relevant experiments. Hector has the ability to be a key analytical tool used across many scientific and policy communities due to its modern software architecture, open source, and object-oriented structure.

## Code availabilty

Hector is freely available at https://github.com/JGCRI/hector. The specific Hector v0.1 referenced in this paper is available at https://github.com/JGCRI/hector/releases/tag/v0.1

*Author contributions.* C. A. Hartin and B. P. Bond-Lamberty developed the ocean and terrestrial carbon models, respectively, and led the overall development of Hector. R. P. Link and P. Patel wrote critical code for Hector's coupler and carbon cycle solver. A. Schwarber helped with the development of the atmospheric forcing components. C. A. Hartin wrote the manuscript with contributions from all co-authors.

*Acknowledgements.* This research is based on work supported by the U.S. Department of Energy, Office of Science, Integrated Assessment Research Program. The Pacific Northwest National Laboratory is operated for DOE by Battelle Memorial Institute under contract DE-AC05-76RL01830.

## References

Applegate, P. J., Kirchner, N., Stone, E. J., Keller, K., and Greve, R.: An assessment of key model parametric uncertainties in projections of Greenland Ice Sheet behavior, The Cryosphere, 6, 589–606, doi:10.5194/tc-6-589-2012, 2012.

Bates, N. R.: Interannual variability of the oceanic CO2 sink in the subtropical gyre of the North Atlantic Ocean over the last 2 decades, J. Geophys. Res.-Oceans, 112, C09013, doi:10.1029/2006JC003759, 2007.

Bond, T. C., Doherty, S. J., Fahey, D. W., Forster, P. M., Berntsen, T., DeAngelo, B. J., Flanner, M. G., Ghan, S., Kärcher, B., Koch, D., Kinne, S., Kondo, Y., Quinn, P. K., Sarofim, M. C., Schultz, M. G., Schulz, M., Venkataraman, C., Zhang, H., Zhang, S., Bellouin, N., Guttikunda, S. K., Hopke, P. K., Jacobson, M. Z., Kaiser, J. W., Klimont, Z., Lohmann, U., Schwarz, J. P., Shindell, D., Storelvmo, T., Warren, S. G., and Zender, C. S.: Bounding the role of black carbon in the climate system: a scientific assessment, J. Geophys. Res.-Atmos., 118, 5380–5552, doi:10.1002/jgrd.50171, 2013.

Challenor, P.: Using emulators to estimate uncertainty in complex models, Uncertainty Quantification in Scientific Computing, 377, 151–164, 2012.

Edmonds, J. and Smith, S. J.: The Technology of Two Degrees. Avoiding Dangerous Climate Change, edited by: Schellnhuber, H. J., Cramer, W., Nakicenovic, N., Wigley, T., and Yohe, G., Cambridge University Press, Cambridge, UK, 2006.

Ehhalt, D., Prather, M. J., Dentener, F. J., Derwent, R., Dlugokencky, E. J., Holland, E. A., Isaksen, I. S., Katima, J., Kirchoff, V., Matson, P. A., and Wang, M.: Atmospheric chemistry and greenhouse gases, in: Climate Change 2001: The Scientific Basis, edited by: Houghton, J. T., Ding, Y., Griggs, D. J., Noguer, M., van der Linden, L., Dai, X., Maskell, K., and Johnson, C. A., Cambridge University Press, Cambridge, UK, 892, 2001.

Etheridge, D. M., Steele, L. P., Langenfelds, R. L., Francey, R. J., Barnola, J. M., and Morgan, V. I.: Natural and anthropogenic changes in atmospheric CO2 over the last 1000 years from air in Antarctic ice and firn, J. Geophys. Res.-Atmos., 101, 4115–4128, doi:10.1029/95JD03410, 1996.

Friedlingstein, P., Meinshausen, M., Arora, V. K., Jones, C. D., Anav, A., Liddicoat, S. K., and Knutti, R.: Uncertainties in CMIP5 climate projections due to carbon cycle feedbacks, J. Climate, 27, 511–526, doi:10.1175/JCLI-D-12-00579.1, 2014.

Fujieki, L., Santiago-Mandujano, F., Fumar, C., Liukas, R., and Church, M.: Hawaii Ocean Time-series Program Data Report, 2013.

Hartin, C. A., Bond-Lamberty, B., and Patel, P.: Projections of ocean acidification over three centuries using a carbonate chemsitry box model, Biogeosciences Discuss., in preparation, 2014.

Harvey, L. D. D. and Schneider, S. H.: Transient climate response to external forcing on 100–104 year time scales part 1: Experiments with globally averaged, coupled, atmosphere and ocean energy balance models, J. Geophys. Res.-Atmos., 90, 2191–2205, doi:10.1029/JD090iD01p02191, 1985.

Heron, M., Hanson, V., and Ricketts, I.: Open source and accessibility: advantages and limitations, Journal of Interaction Science, 1, doi:10.1186/2194-0827-1-2, 2013.





GMDD
7, 7075–7119, 2014

A simple open source model for analyses of the global carbon cycle – Hector v0.1

C. A. Hartin et al.

Hoffert, M. I., Callegari, A. J., and Hsieh, C.-T.: The role of deep sea heat storage in the secular response to climatic forcing, J. Geophys. Res., 85, 6667–6679, doi:10.1029/JC085iC11p06667, 1980.
Ince, D. C., Hatton, L., and Graham-Cumming, J.: The case for open computer programs, Nature, 482, 485–488, 2012.
IPCC: Climate Change 2001: The Science of Climate Change. Contribution of Working Group I to the Second Assessment Report of the Intergovernmental Panel on Climate Change, Cambridge University Press, Cambridge, , 2001.
Irvine, P. J., Sriver, R. L., and Keller, K.: Tension between reducing sea-level rise and global warming through solar-radiation management, Nature Clim. Change, 2, 97–100, 2012.
Joos, F., Prentice, I. C., Sitch, S., Meyer, R., Hooss, G., Plattner, G.-K., Gerber, S., and Hasselmann, K.: Global warming feedbacks on terrestrial carbon uptake under the Intergovernmental Panel on Climate Change (IPCC) Emission Scenarios, Global Biogeochem. Cy., 15, 891–907, doi:10.1029/2000GB001375, 2001.
Knox, F. and McElroy, M. B.: Changes in atmospheric $CO_2$: influence of the marine biota at high latitude, J. Geophys. Res., 89, 4629–4637, doi:10.1029/JD089iD03p04629, 1984.
Knutti, R. and Hegerl, G. C.: The equilibrium sensitivity of the Earth's temperature to radiation changes, Nat. Geosci., 1, 735–743, 2008.
Le Quéré, C., Andres, R. J., Boden, T., Conway, T., Houghton, R. A., House, J. I., Marland, G., Peters, G. P., van der Werf, G. R., Ahlström, A., Andrew, R. M., Bopp, L., Canadell, J. G., Ciais, P., Doney, S. C., Enright, C., Friedlingstein, P., Huntingford, C., Jain, A. K., Jourdain, C., Kato, E., Keeling, R. F., Klein Goldewijk, K., Levis, S., Levy, P., Lomas, M., Poulter, B., Raupach, M. R., Schwinger, J., Sitch, S., Stocker, B. D., Viovy, N., Zaehle, S., and Zeng, N.: The global carbon budget 1959–2011, Earth Syst. Sci. Data, 5, 165–185, doi:10.5194/essd-5-165-2013, 2013.
Lenton, T. M.: Land and ocean carbon cycle feedback effects on global warming in a simple Earth system model, Tellus B, 52, 1159–1188, doi:10.1034/j.1600-0889.2000.01104.x, 2000.
Martin, R. C., Riehle, D., and Buschmann, F.: Pattern Languages of Program Design 3, Addison-Wesley, Boston, MA, 672 pp., 1997.
Masui, T., Matsumoto, K., Hijioka, Y., Kinoshita, T., Nozawa, T., Ishiwatari, S., Kato, E., Shukla, P. R., Yamagata, Y., and Kainuma, M.: An emission pathway for stabilization at 6 Wm-2 radiative forcing, Climatic Change, 109, 59–76, doi:10.1007/s10584-011-0150-5, 2011.





GMDD
7, 7075–7119, 2014

A simple open source model for analyses of the global carbon cycle – Hector v0.1

C. A. Hartin et al.

Meinshausen, M., Raper, S. C. B., and Wigley, T. M. L.: Emulating coupled atmosphere-ocean and carbon cycle models with a simpler model, MAGICC6 – Part 1: Model description and calibration, Atmos. Chem. Phys., 11, 1417–1456, doi:10.5194/acp-11-1417-2011, 2011a.
Meinshausen, M., Smith, S. J., Calvin, K., Daniel, J. S., Kainuma, M. L. T., Lamarque, J. F., Matsumoto, K., Montzka, S. A., Raper, S. C. B., Riahi, K., Thomson, A., Velders, G. J. M., and Vuuren, D. P. P.: The RCP greenhouse gas concentrations and their extensions from 1765 to 2300, Climatic Change, 109, 213–241, doi:10.1007/s10584-011-0156-z, 2011b.
Meinshausen, M., Wigley, T. M. L., and Raper, S. C. B.: Emulating atmosphere-ocean and carbon cycle models with a simpler model, MAGICC6 – Part 2: Applications, Atmos. Chem. Phys., 11, 1457–1471, doi:10.5194/acp-11-1457-2011, 2011c.
Morice, C. P., Kennedy, J. J., Rayner, N. A., and Jones, P. D.: Quantifying uncertainties in global and regional temperature change using an ensemble of observational estimates: the HadCRUT4 data set, J. Geophys. Res.-Atmos., 117, D08101, doi:10.1029/2011JD017187, 2012.
Moss, R. H., Edmonds, J. A., Hibbard, K. A., Manning, M. R., Rose, S. K., van Vuuren, D. P., Carter, T. R., Emori, S., Kainuma, M., Kram, T., Meehl, G. A., Mitchell, J. F. B., Nakicenovic, N., Riahi, K., Smith, S. J., Stouffer, R. J., Thomson, A. M., Weyant, J. P., and Wilbanks, T. J.: The next generation of scenarios for climate change research and assessment, Nature, 463, 747–756, 2010.
Piao, S., Sitch, S., Ciais, P., Friedlingstein, P., Peylin, P., Wang, X., Ahlström, A., Anav, A., Canadell, J. G., Cong, N., Huntingford, C., Jung, M., Levis, S., Levy, P. E., Li, J., Lin, X., Lomas, M. R., Lu, M., Luo, Y., Ma, Y., Myneni, R. B., Poulter, B., Sun, Z., Wang, T., Viovy, N., Zaehle, S., and Zeng, N.: Evaluation of terrestrial carbon cycle models for their response to climate variability and to CO2 trends, Glob. Change Biol., 19, 2117–2132, doi:10.1111/gcb.12187, 2013.
Pietsch, S. A. and Hasenauer, H.: Evaluating the self-initialization procedure for large-scale ecosystem models, Glob. Change Biol., 12, 1–12, doi:10.1111/j.1365-2486.2006.01211.x, 2006.
Raper, S. C., Gregory, J. M., and Stouffer, R. J.: The role of climate sensititivity and ocean heat uptake on AOGCM transient temperature response, J. Climate, 15, 124–130, 2002.
Raper, S. C. B., Gregory, J. M., and Osborn, T. J.: Use of an upwelling-diffusion energy balance climate model to simulate and diagnose A/O GCM results, Clim. Dynam., 17, 601–613, 2001.

Ratto, M., Castelletti, A., and Pagano, A.: Emulation techniques for the reduction and sensitivity analysis of complex environmental models, Environ. Modell. Softw., 34, 1–4, 2012.
Riahi, K., Rao, S., Krey, V., Cho, C., Chirkov, V., Fischer, G., Kindermann, G., Nakicenovic, N., and Rafaj, P.: RCP 8.5 – a scenario of comparatively high greenhouse gas emissions, Climatic Change, 109, 33–57, doi:10.1007/s10584-011-0149-y, 2011.
Ricciuto, D. M., Davis, K. J., and Keller, K.: A Bayesian calibration of a simple carbon cycle model: the role of observations in estimating and reducing uncertainty, Global Biogeochem. Cy., 22, GB2030, doi:10.1029/2006GB002908, 2008.
Schlesinger, M. E. and Jiang, X.: Simple model representation of atmosphere–ocean GCMs and estimation of the time scale of $CO_2$-induced climate change, J. Climate, 3, 1297–1315, doi:10.1175/1520-0442(1990)003<1297:SMROAO>2.0.CO;2, 1990.
Senior, C. A. and Mitchell, J. F. B.: The time-dependence of climate sensitivity, Geophys. Res. Lett., 27, 2685–2688, doi:10.1029/2000GL011373, 2000.
Smith, S. J. and Bond, T. C.: Two hundred fifty years of aerosols and climate: the end of the age of aerosols, Atmos. Chem. Phys., 14, 537–549, doi:10.5194/acp-14-537-2014, 2014.
Sriver, R., Urban, N., Olson, R., and Keller, K.: Toward a physically plausible upper bound of sea-level rise projections, Climatic Change, 115, 893–902, doi:10.1007/s10584-012-0610-6, 2012.
Stocker, T.: Model hierarchy and simplified climate models, in: Introduction to Climate Modelling, Advances in Geophysical and Environmental Mechanics and Mathematics, Springer, Berlin, Heidelberg, 25–51, 2011.
Takahashi, T., Sutherland, S. C., Wanninkhof, R., Sweeney, C., Feely, R. A., Chipman, D. W., Hales, B., Friederich, G., Chavez, F., Sabine, C., Watson, A., Bakker, D. C. E., Schuster, U., Metzl, N., Yoshikawa-Inoue, H., Ishii, M., Midorikawa, T., Nojiri, Y., Körtzinger, A., Steinhoff, T., Hoppema, M., Olafsson, J., Arnarson, T. S., Tilbrook, B., Johannessen, T., Olsen, A., Bellerby, R., Wong, C. S., Delille, B., Bates, N. R., and de Baar, H. J. W.: Climatological mean and decadal change in surface ocean pCO2, and net sea–air $CO_2$ flux over the global oceans, Deep-Sea Res. Pt. II, 56, 554–577, doi:10.1016/j.dsr2.2008.12.009, 2009.
Tanaka, K., Kriegler, E., Bruckner, T., Hooss, C., Knorr, W., and Raddatz, T.: Aggregated Carbon Cycle, Atmospheric Chemistry, and Climate Model (ACC2) – Description of the Forward and Inverse Models, Max Planck Institute for Meteorology, Hamburg, Germany, 188 pp., 2007a.





GMDD
7, 7075–7119, 2014



Title Page
Abstract | Introduction
Conclusions | References
Tables | Figures
◂◂ | ▸▸
◂ | ▸
Back | Close
Full Screen / Esc
Printer-friendly Version
Interactive Discussion

Tanaka, K., Kriegler, E., Bruckner, T., Hooss, G., Knorr, W., Raddatz, T. J., and Tol, R.: Aggregated Carbon Cycle, Atmospheric Chemistry, and Climate Model (ACC2), Hamburg, 188, 2007b.
Taylor, K. E., Stouffer, R. J., and Meehl, G. A.: An Overview of CMIP5 and the Experiment Design, B. Am. Meteorol. Soc., 93, 485–498, doi:10.1175/BAMS-D-11-00094.1, 2012.
Thomson, A., Calvin, K., Smith, S., Kyle, G. P., Volke, A., Patel, P., Delgado-Arias, S., Bond-Lamberty, B., Wise, M., Clarke, L., and Edmonds, J.: RCP4.5: a pathway for stabilization of radiative forcing by 2100, Climatic Change, 109, 77–94, doi:10.1007/s10584-011-0151-4, 2011.
Urban, N. M. and Keller, K.: Complementary observational constraints on climate sensitivity, Geophys. Res. Lett., 36, L04708, doi:10.1029/2008GL036457, 2009.
van Vuuren, D., Edmonds, J., Kainuma, M., Riahi, K., Thomson, A., Hibbard, K., Hurtt, G., Kram, T., Krey, V., Lamarque, J.-F., Masui, T., Meinshausen, M., Nakicenovic, N., Smith, S., and Rose, S.: The representative concentration pathways: an overview, Climatic Change, 109, 5–31, doi:10.1007/s10584-011-0148-z, 2011a.
van Vuuren, D., Edmonds, J., Kainuma, M., Riahi, K., and Weyant, J.: A special issue on the RCPs, Climatic Change, 109, 1–4, doi:10.1007/s10584-011-0157-y, 2011b.
van Vuuren, D., Lowe, J., Stehfest, E., Gohar, L., Hof, A., Hope, C., Warren, R., Meinshausen, M., and Plattner, G.-K.: How well do integrated assessment models simulate climate change?, Climatic Change, 104, 255–285, doi:10.1007/s10584-009-9764-2, 2011c.
van Vuuren, D., Stehfest, E., den Elzen, M. J., Kram, T., van Vliet, J., Deetman, S., Isaac, M., Klein Goldewijk, K., Hof, A., Mendoza Beltran, A., Oostenrijk, R., and van Ruijven, B.: RCP2.6: exploring the possibility to keep global mean temperature increase below 2 °C, Climatic Change, 109, 95–116, doi:10.1007/s10584-011-0152-3, 2011d.
White, E. P., Baldridge, E., Brym, Z. T., Locey, K. J., McGlinn, D. J., and Supp, S. R.: Nine simple ways to make it easier to (re)use your data, Peer J. PrePrints, 1:e7v2, doi:10.7287/peerj.preprints.7v2, 2013.
Wigley, T. M. L.: A simple inverse carbon cycle model, Global Biogeochem. Cy., 5, 373–382, doi:10.1029/91GB02279, 1991.
Wigley, T. M. L.: Global-mean temperature and sea level consequences of greenhouse gas concentration stabilization, Geophys. Res. Lett., 22, 45–48, doi:10.1029/94GL01011, 1995.
Wigley, T. M. L., Richels, R., and Edmonds, J. A.: Economic and environmental choices in the stabilization of atmospheric $CO_2$ concentrations, Nature, 379, 240–243, 1996.





GMDD
7, 7075–7119, 2014
A simple open source model for analyses of the global carbon cycle – Hector v0.1
C. A. Hartin et al.

Zeebe, R. E. and Wolf-Gladrow, D.: $CO_2$ in Seawater: Equilibrium, Kinetics, Isotopes, Elsevier, 2001.





GMDD
7, 7075–7119, 2014

A simple open source model for analyses of the global carbon cycle – Hector v0.1

C. A. Hartin et al.

**Table 1.** Initial model conditions prior to spinup, assuming a pre-industrial steady state.

| Variable | Description | Initial value | Units |
|---|---|---|---|
| $C_{atm}$ * | Atmospheric Carbon | 588.1 | Pg C |
| $C_D$ * | Detritus Carbon | 55 | Pg C |
| $C_S$ * | Soil Carbon | 1782 | Pg C |
| $C_V$ * | Vegetation Carbon | 550 | Pg C |
| $C_{DO}$ | Deep Ocean | 26 000 | Pg C |
| $C_{HL}$ | Surface Ocean High Latitude | 140 | Pg C |
| $C_{IO}$ | Intermediate Ocean | 8400 | Pg C |
| $C_{LL}$ | Surface Ocean Low Latitude | 770 | Pg C |
| $F_L$ | Atmosphere–Land Carbon Flux | 0 | $Pg C yr^{-1}$ |
| $F_O$ | Atmosphere–Ocean Carbon Flux | 0 | $Pg C yr^{-1}$ |
| $NPP_0$ | Net Primary Production | 50 | $Pg C yr^{-1}$ |
| $T_G$ | Global Temperature Anomaly | 0 | °C |
| $T_{HL}$ | Temperature of high latitude surface ocean box | 2 | °C |
| $T_{LL}$ | Temperature of low latitude surface ocean box | 22 | °C |

* Parameters appearing in the input file.





GMDD
7, 7075–7119, 2014

**Table 2.** Model parameters for the land and ocean carbon components.

| Variable | Description | Value |
|---|---|---|
| $f_{ds}$ | annual fraction of detritus carbon that is transferred to soil | 0.60 |
| $f_{ld}$ * | annual fraction of land use change flux from detritus | 0.01 |
| $f_{ls}$ | annual fraction of land use change flux from soil | 0.89 |
| $f_{lv}$ * | annual fraction of land use change flux from vegetation | 0.10 |
| $f_{nd}$ * | annual fraction of NPP carbon that is transferred to detritus | 0.60 |
| $f_{ns}$ | annual fraction of NPP carbon that is transferred to soil | 0.05 |
| $f_{nv}$ * | annual fraction of NPP carbon that is transferred to vegetation | 0.35 |
| $f_{rd}$ | annual fraction of respiration carbon that is transferred to detritus | 0.25 |
| $f_{rs}$ | annual fraction of respiration carbon that is transferred to soil | 0.02 |
| $f_{vd}$ | annual fraction of vegetation carbon that is transferred to detritus | 0.034 |
| $f_{vs}$ | annual fraction of vegetation carbon that is transferred to soil | 0.001 |
| $\beta$ * | Beta | 0.36 |
| $Q10$ * | $Q10$ respiration | 2.45 |
| $T_H$ * | High-latitude circulation | 4.9e7 $m^3 s^{-1}$ |
| $T_T$ * | Thermohaline circulation | 7.2e7 $m^3 s^{-1}$ |
| $E_{ID}$ * | Water mass exchange – intermediate – deep | 1.25e7 $m^3 s^{-1}$ |
| $E_{LI}$ * | Water mass exchange – low latitude – intermediate | 2.0e8 $m^3 s^{-1}$ |

* Parameters appearing in the input file.





GMDD
7, 7075–7119, 2014

**Table 3.** CMIP5 ESM models used within this study. We use the same suite of models as found in Friedlingstein et al. (2014). Note, not all variables are reported for each model under all scenarios.

| Model | Model name | Institute |
|---|---|---|
| bcc-csm1-1 | Beijing Climate Center, Climate System Model, version 1.1 | Beijing Climate Center, China Meteorological Administration, China |
| CanESM2 | Second Generation Canadian Earth System Model | Canadian Center for Climate Modeling and Analysis, BC, Canada |
| CESM1-BGC | Community Earth System Model, version 1.0-Biogeochemistry | National Center for Atmospheric Research, United States |
| GFDL-ESM2G | Geophysical Fluid Dynamic Laboratory Earth System Model with GOLD ocean component | Geophysical Fluid Dynamics Laboratory, United States |
| HadGEM2-ES | Hadley Centre Global Environmental Model, version 2 (Earth System) | Met Office Hadley Centre, UK |
| inmcm4 | Institute of Numerical Mathematics Coupled Model, version 4.0 | Institute of Numerical Mathematics, Russia |
| IPSL-CM5A-LR | L'Institut Pierre-Simon Laplace Coupled Model, version 5A, coupled with NEMO, low resolution | Institut Pierre Simon Laplace, France |
| MIROC-ESM | Model for Interdisciplinary Research on Climate, Earth System Model | Atmosphere and Ocean Research Institute; National Institute for Environmental Studies, Japan Agency for Marine-Earth Science and Technology, Japan |
| MPI-ESM-LR | Max Planck Institute Earth System Model, low resolution | Max Planck Institute for Meteorology, Germany |
| MRI-ESM1 | Meteorological Research Institute Earth System Model, version 1 | Meteorological Research Institute Earth, Japan |
| NorESM1-ME | Norwegian Earth System Model, version 1, intermediate resolution | Norwegian Climate Center, Norway |





GMDD
7, 7075–7119, 2014

**Table 4a.** Skill of Hector vs. observations, CMIP5, and MAGICC, correlation coefficients (*R*) and root mean square error (RMSE) for atmospheric [$CO_2$], surface temperature anomaly, radiative forcing, fluxes of carbon (ocean and land), and low latitude surface ocean pH.

| Historical 1850–2004 | | | | | |
|---|---|---|---|---|---|
| Variable | Skill | observations | MAGICC | CMIP5 | Units |
| [$CO_2$]* | *R* | 0.99 | 0.99 | 1.0 | ppmv |
| | RMSE | 2.73 | 2.84 | 2.11 | |
| temperature | *R* | 0.85 | 0.85 | 0.81 | deg C |
| | RMSE | 0.11 | 0.11 | 0.13 | |
| Forcing | *R* | – | 0.79 | – | $W m^{-2}$ |
| | RMSE | – | 0.36 | – | |
| Ocean Flux | *R* | – | – | 0.95 | $Pg C yr^{-1}$ |
| | RMSE | – | – | 0.27 | |
| Land Flux | *R* | – | – | 0.55 | $Pg C yr^{-1}$ |
| | RMSE | – | – | 1.30 | |
| pH | *R* | | – | 0.99 | unitless |
| | RMSE | | – | 0.003 | |

* [$CO_2$] observations are an average of Law Dome and Mauna Loa.





GMDD
7, 7075–7119, 2014
A simple open source model for analyses of the global carbon cycle – Hector v0.1
C. A. Hartin et al.

**Table 4b.** Continued.

| RCP 8.5 1850–2300 | | | | |
|---|---|---|---|---|
| Variable | Skill | MAGICC | CMIP5 | Units |
| $[CO_2]$ | *R* | 1.0 | 0.99 | ppmv |
| | RMSE | 7.69 | 10.62 | |
| temperature | *R* | 1.0 | 0.98 | °C |
| | RMSE | 0.33 | 0.91 | |
| Forcing | *R* | 1.0 | – | $W\,m^{-2}$ |
| | RMSE | 0.25 | – | |
| Ocean Flux | *R* | | 0.80 | $Pg\,C\,yr^{-1}$ |
| | RMSE | | 1.45 | |
| Land Flux | *R* | – | 0.60 | $Pg\,C\,yr^{-1}$ |
| | RMSE | – | 4.01 | |
| pH | *R* | – | 1 | unitless |
| | RMSE | – | 0.004 | |

* CMIP5 $[CO_2]$ only to 2100.





GMDD
7, 7075–7119, 2014
A simple open source model for analyses of the global carbon cycle – Hector v0.1
C. A. Hartin et al.

**Table 4c.** Continued.

| RCP 8.5 2005–2300 | | | | |
|---|---|---|---|---|
| Variable | Skill | MAGICC | CMIP5 | Units |
| $[CO_2]^*$ | *R* | 1.0 | 1.0 | ppmv |
| | RMSE | 8.64 | 10.23 | |
| temperature | *R* | 1.0 | 0.97 | °C |
| | RMSE | 0.17 | 0.86 | |
| Forcing | *R* | 1.0 | – | $W\,m^{-2}$ |
| | RMSE | 0.04 | – | |
| Ocean Flux | *R* | – | 0.10 | $Pg\,C\,yr^{-1}$ |
| | RMSE | – | 1.42 | |
| Land Flux | *R* | – | 0.65 | $Pg\,C\,yr^{-1}$ |
| | RMSE | – | 4.73 | |
| pH | *R* | – | 1.0 | unitless |
| | RMSE | – | 0.003 | |

* CMIP5 $[CO_2]$ only to 2100.





GMDD
7, 7075–7119, 2014

A simple open source model for analyses of the global carbon cycle – Hector v0.1

C. A. Hartin et al.

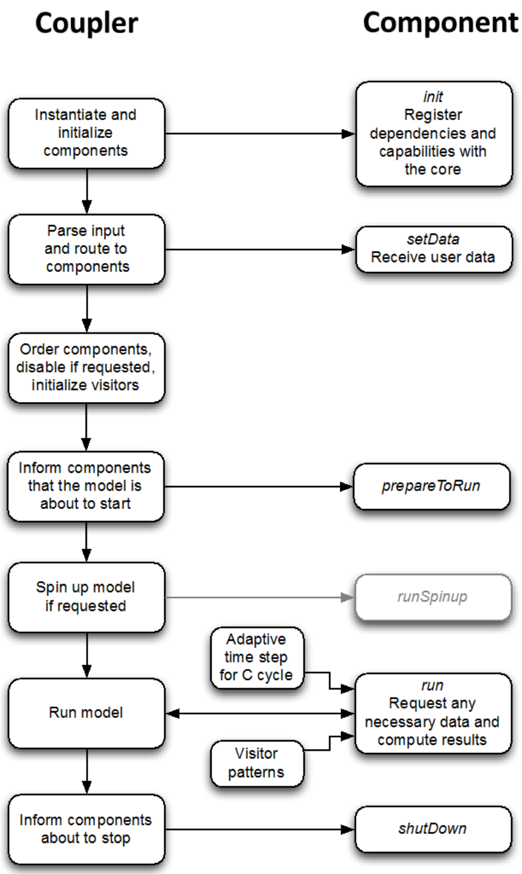


**Figure 1.** Model phases for the coupler (left) and a typical component (right). Arrows show flow of control and data. The greyed spinup step is optional.





GMDD
7, 7075–7119, 2014

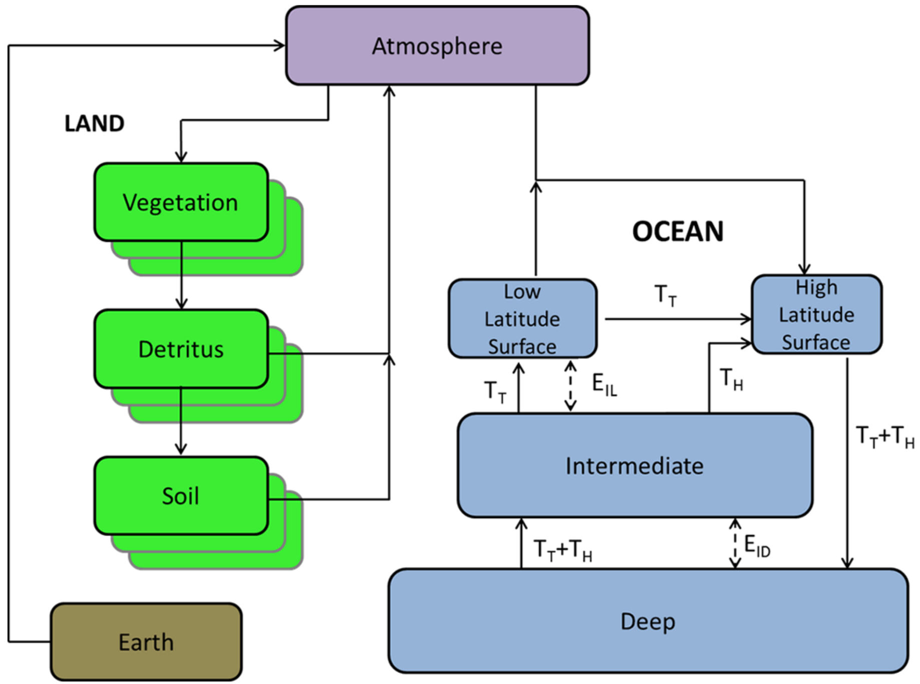


**Figure 2.** Representation of Hector's carbon cycle, land, atmosphere, and ocean. The atmosphere consists of one well mixed box. The ocean consists of four boxes, with advection and water mass exchange simulating thermohaline circulation. At steady state, the high latitude surface ocean takes up carbon from the atmosphere, while the low latitude surface ocean off gases carbon to the atmosphere. The land consists of a user defined number of biomes or regions for vegetation, detritus and soil. At steady state the vegetation takes up carbon from the atmosphere while the detritus and soil release carbon back into the atmosphere. The earth pool is continually debited with each time step to act as a mass balance check on the carbon system.





GMDD
7, 7075–7119, 2014

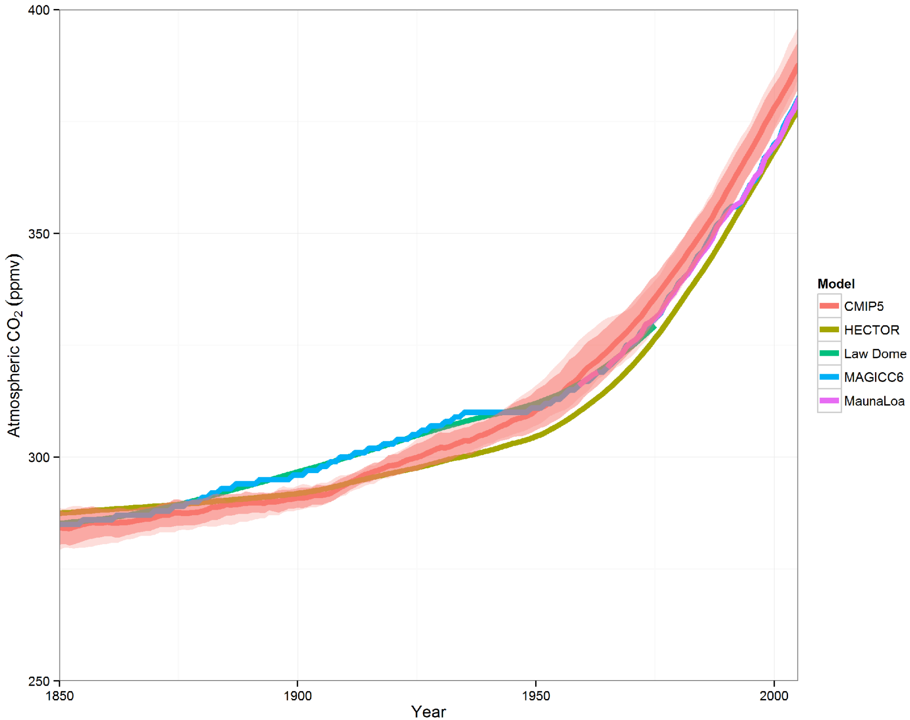


**Figure 3.** Historical atmospheric [$CO_2$] from 1850 to 2005 for Hector (brown), CMIP5 (pink), MAGICC6 (blue), Law Dome (green), and Mauna Loa (purple). Note CMIP5 data are from the emissions driven historical scenario (esmHistorical). Notice that MAGICC6 matches the observational record. We have the capabilities of running Hector under numerous constraints. Within this study we are running Hector unconstrained to highlight the full performance of the model.





GMDD
7, 7075–7119, 2014

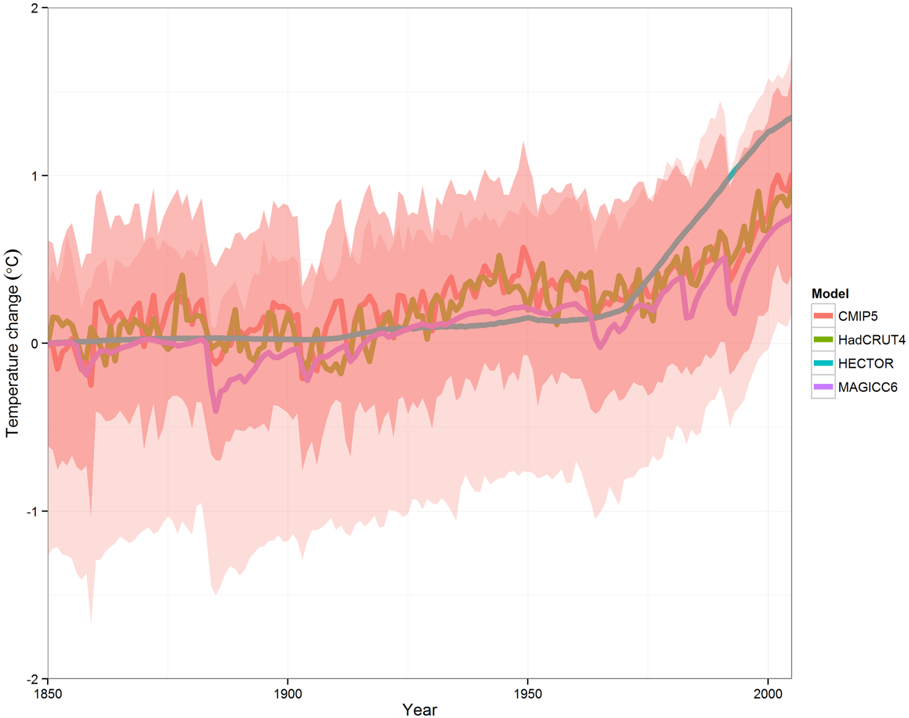


**Figure 4.** Historical global temperature anomaly relative to 1850 for Hector (blue), MAGICC6 (purple), CMIP5 median, SD and model spread (pink), and historical observations from HadCRUT4 (green).





GMDD
7, 7075–7119, 2014

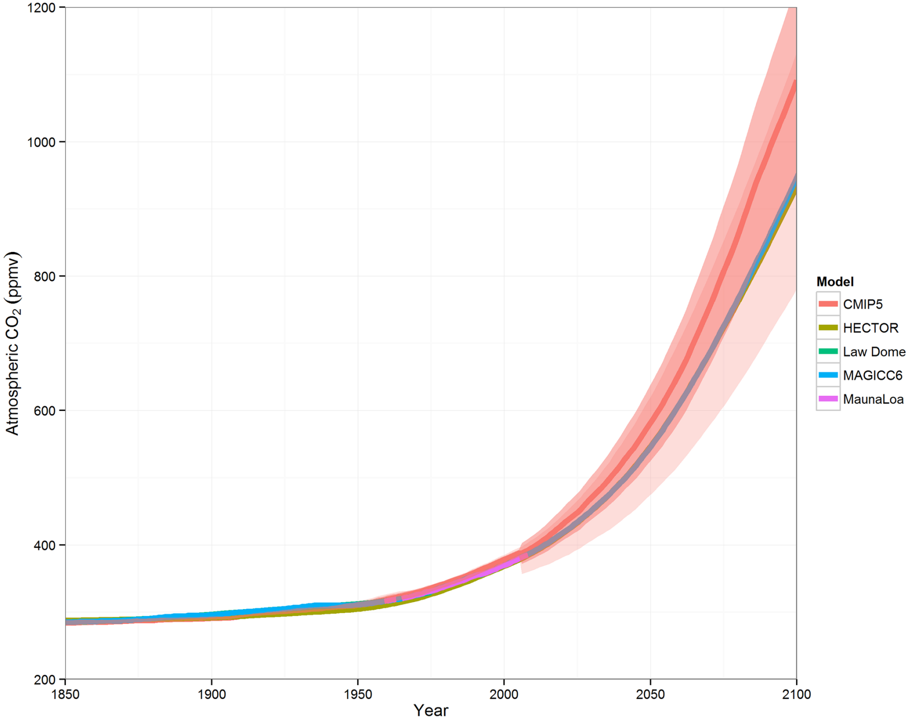


**Figure 5.** Atmospheric [$CO_2$] from 1850 to 2100 under RCP 8.5 for Hector (yellow), MAGICC6 (blue), Mauna Loa (purple), Law Dome (green) and esmRCP 8.5 CMIP5 median, one SD and model spread (pink).





GMDD
7, 7075–7119, 2014

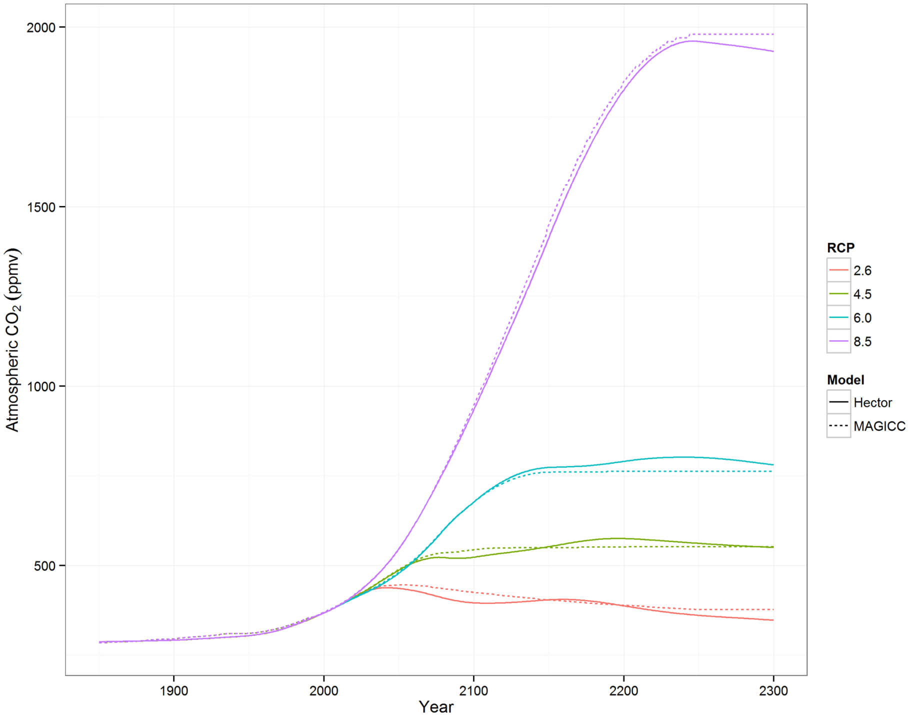


**Figure 6.** Atmospheric [$CO_2$] from 1850 to 2300 for RCP 2.6 (yellow), RCP 4.5 (green), RCP 6.0 (blue), RCP 8.5 (purple), Hector (solid) and MAGICC6 (dashed).

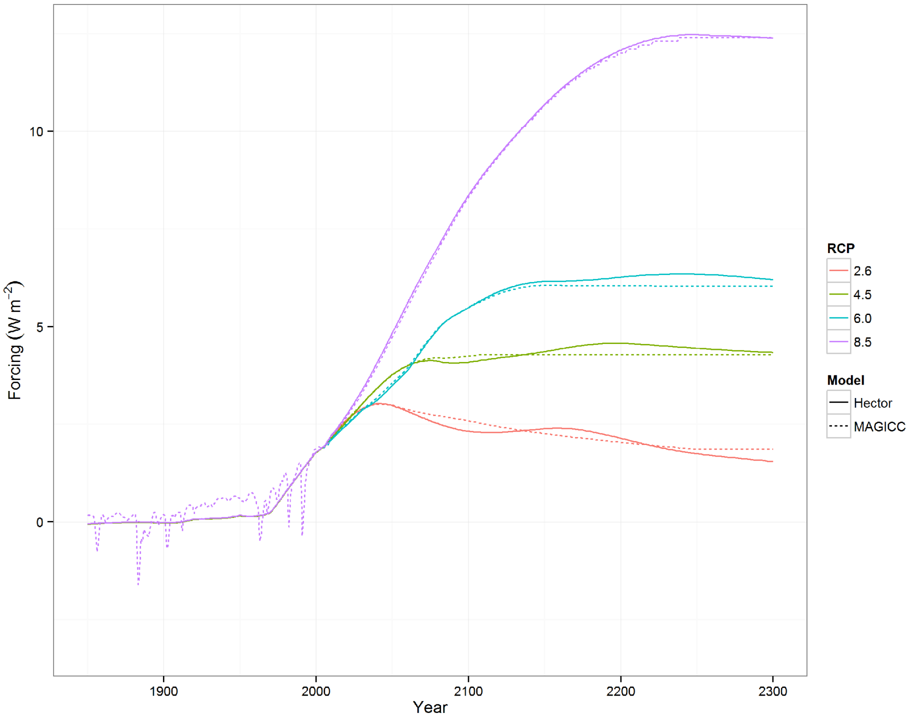


**Figure 7.** Relative radiative forcing from 1850 to 2300 for Hector (solid) and MAGICC6 (dashed) for all four RCP scenarios, 2.6 (red), 4.5 (green), 6.0 (blue), 8.5 (purple). Hector has the option to enable or disable radiative forcing from historical volcanic emissions. We have opted to disable this for ease of comparison across all RCPs.





GMDD
7, 7075–7119, 2014

A simple open source model for analyses of the global carbon cycle – Hector v0.1

C. A. Hartin et al.

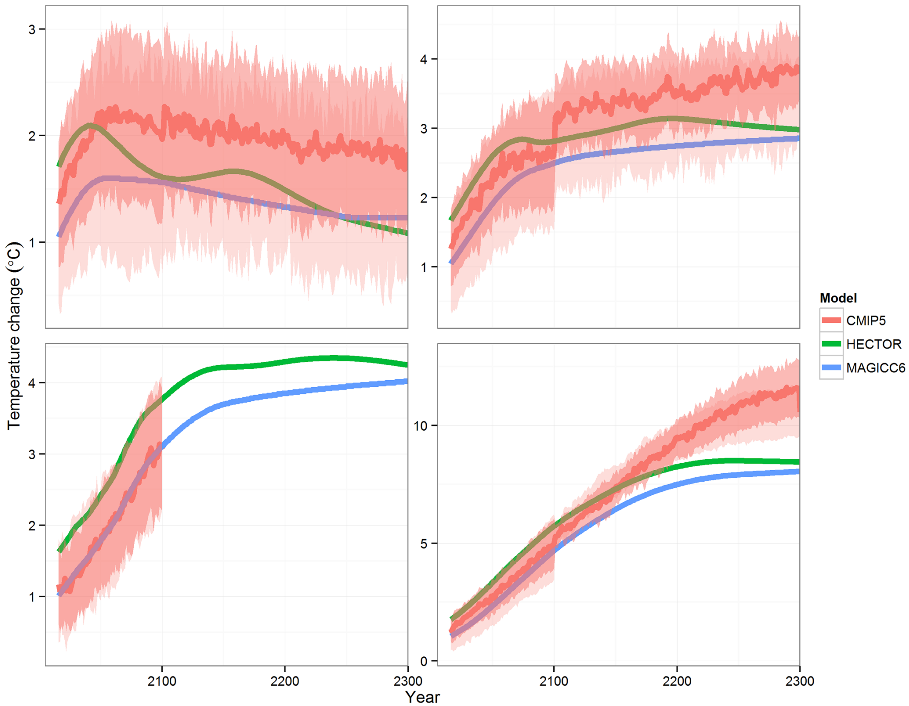


**Figure 8.** Global temperature anomaly relative to 1850 for **(a)** RCP 2.6, **(b)** RCP 4.5, **(c)** RCP 6.0, and **(d)** RCP 8.5, comparing Hector (green), MAGICC6 (blue), and CMIP5 median, SD and model spread (pink). The CMIP5 models under RCP 6.0 used in this study do not extend to 2300. Note the change in scales between the four panels.

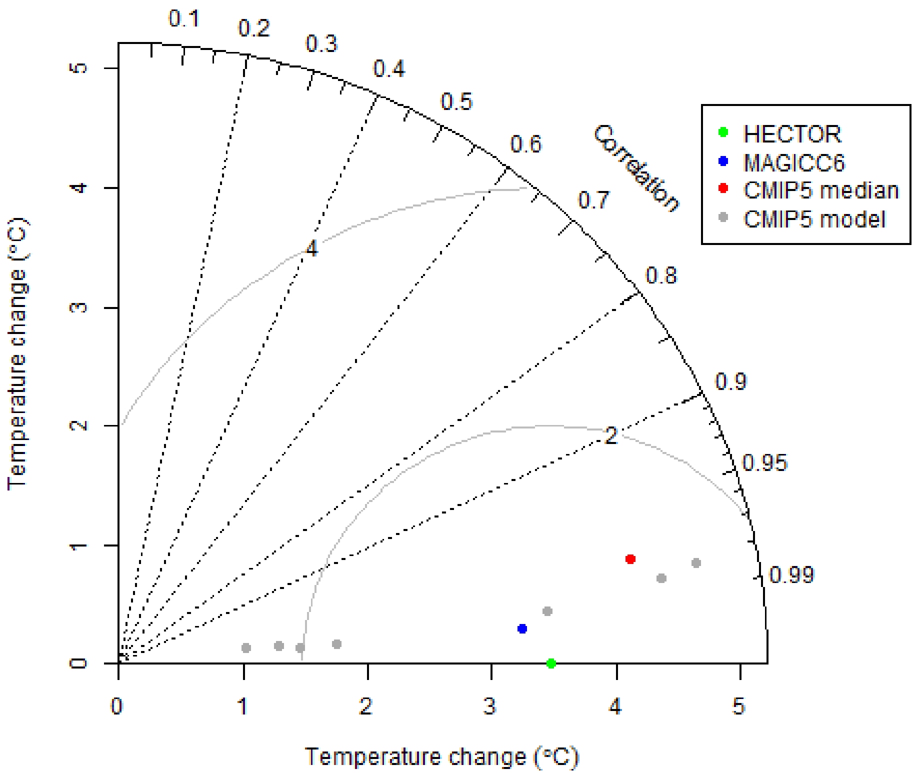


**Figure 9.** Taylor diagram of global temperature anomaly relative to 1850, from 1850 to 2300 for RCP 8.5, Hector (green), MAGICC6 (blue), CMIP5 median (red), and CMIP5 models (grey).





GMDD
7, 7075–7119, 2014

A simple open source model for analyses of the global carbon cycle – Hector v0.1

C. A. Hartin et al.

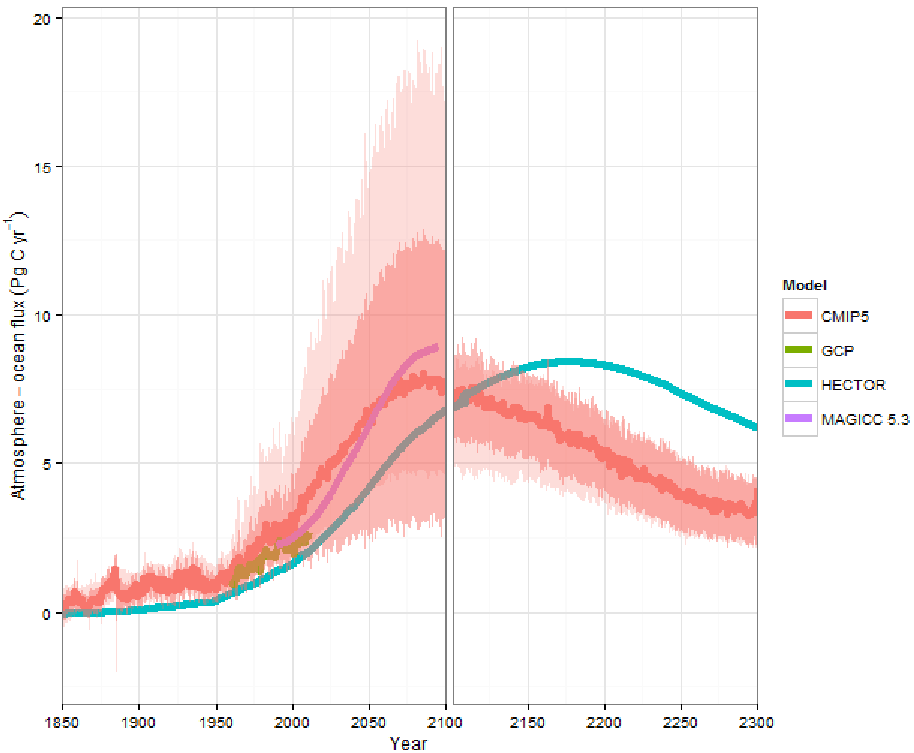


**Figure 10.** Global air-sea fluxes of carbon under RCP 8.5, Hector (blue), MAGICC5.3 (purple, note that this is not the current version of MAGICC), CMIP5 (red), and observations from GCP (Le Quéré et al., 2013). The break in the graph at 2100 signifies a change in the number of models that ran the RCP 8.5 extension.





GMDD
7, 7075–7119, 2014

A simple open source model for analyses of the global carbon cycle – Hector v0.1

C. A. Hartin et al.

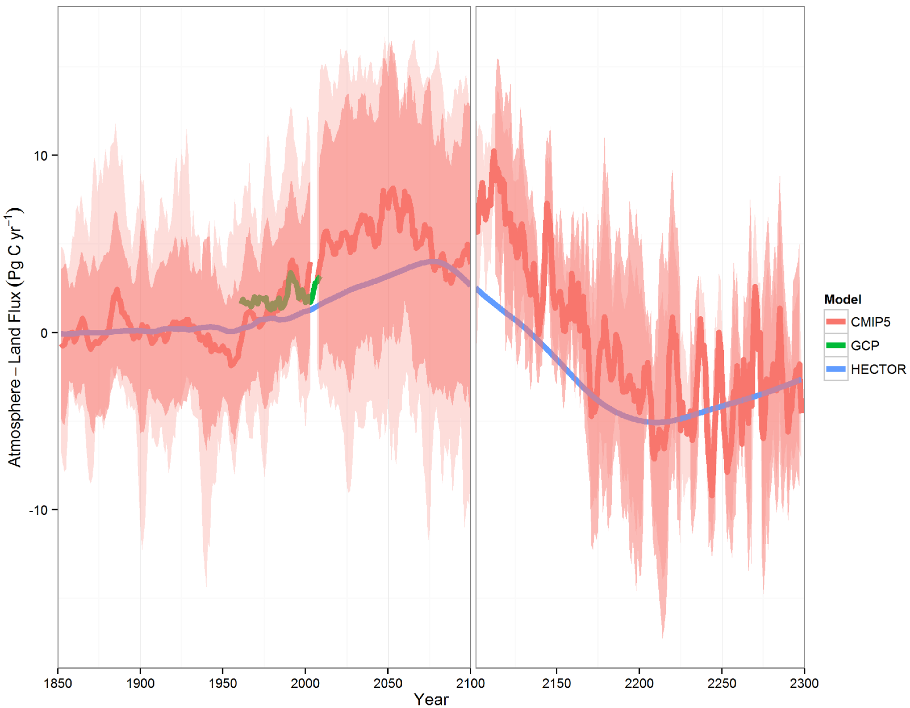


**Figure 11.** Global air–land fluxes of carbon under RCP 8.5, Hector (blue), CMIP5 (red), and observations from GCP (green) (Le Quéré et al., 2013). The break in the graph at 2100 signifies a change in the number of models that ran the RCP 8.5 extension.





GMDD
7, 7075–7119, 2014

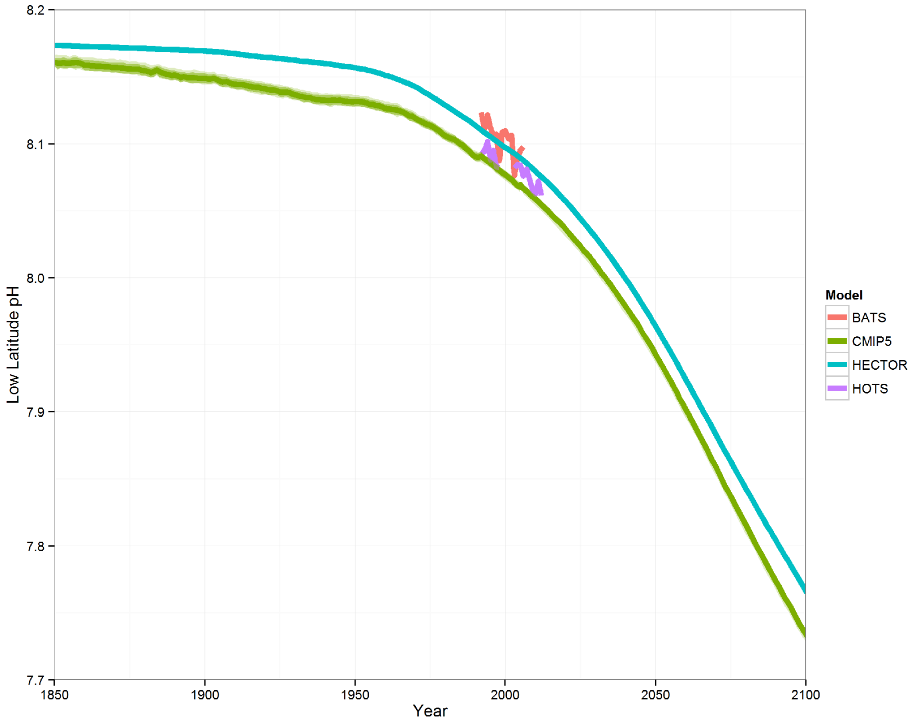


**Figure 12.** Low latitude (< 55) ocean pH for RCP 8.5, from 1850–2100, Hector (blue), CMIP5 (green) and observations from BATS (red) and HOTS (purple).





GMDD
7, 7075–7119, 2014

A simple open source model for analyses of the global carbon cycle – Hector v0.1

C. A. Hartin et al.